Vol. 13, No. 37, Winter 2024, pages 69-90

Journal of Analytical and Numerical Methods in Mining Engineering

Journal home page: http://anm.yazd.ac.ir/

Review article

A review on the buried pipeline responses to tunneling-induced ground settlements

Hadi Mahmoudi[1], Ghorban Khandouzi[1], Mohammad Hossein Khosravi[2]*

1- **School of Mining Engineering, College of Engineering, University of Tehran, Tehran, Iran**
2- **Dept. of Mining Engineering, Faculty of Engineering, University of Birjand, Birjand, Iran**

*Corresponding author: E-mail: *mh.khosravi@birjand.ac.ir*
(Received: *September 2023*, Accepted: *January 2024)*

DOI: 10.22034/ANM.2024.20501.1607

Keywords

Urban area
Service infrastructures
Tunneling
Pipelines
Ground settlement

Abstract

The expansion of cities and urban areas has resulted in an increased demand for environmental and economic transport and services infrastructure. Tunneling, as one of mankind's engineering underground constructions, is taking place close to buried and surface structures such as gas, water, and wastewater pipelines. This paper reviews soil-pipe interaction behavior, tunneling-induced ground settlement, governing equations of soil-pipe settlement, the effects of tunnel depth, size, soil relative density, and volume loss on vertical and horizontal displacement, settlement, shear strain, dilation, pipe bending, and gap formation. A comprehensive literature review, analysis of published papers, and investigations were conducted to study the effect of various parameters on pipeline behavior. The results were obtained by studying the effect of tunneling on ground and pipeline settlement, soil-pipe interaction mechanism, and centrifuge physical modeling. The achieved results of investigations show that the settlement profile follows a Gaussian curve with a wider settlement trough in clay compared to sand. When the tunnel and pipeline are perpendicular to each other, maximum bending strain in the pipeline occurs and the pipeline settlement is symmetrical. The friction effect and formation of contraction and expansion zones lead to the difference between soil volume loss near the surface and tunnel volume loss. When the pipe-soil relative stiffness increases, the pipe bending is less than the maximum soil bending. Also, ground settlement, shear strain, pipeline displacement, and pipeline bending are greater in flexible pipes than in rigid pipelines. This is due to the low resistance of flexible pipelines against bending and settlement caused by tunnel excavation. Positive pipeline bending (downward) occurs near the tunnel axis, which is marked by sagging, but negative bending (upward) occurs at a distance from the tunnel axis, which is known as hogging. In twin tunnels, by increasing the tunnel spacing the pipeline settlement profile changes from a V-shape to a U-shape and finally a W-shape. Understanding soil-pipe interaction behavior, tunneling-induced ground settlement, and the effects of different parameters on displacement, strain field, settlement, pipe bending, and gap formation beneath pipelines is crucial for engineers evaluating pipeline behavior. Additionally, comprehending these issues can help designers make informed decisions during tunnel construction.

1. INTRODUCTION

Population growth leads to increased traffic and the need for complex underground systems. Therefore, tunnel excavation in urban areas and construction of underground spaces, such as subway lines and stations are inevitable to solve this problem. The construction of underground spaces is a complex process that is affected by

various geological phenomena. These phenomena change the state of stress in the ground, which can cause ground movement and deformation. Fig. 1 shows an example of ground movements caused by tunneling. The natural and geological structures can affect tunnel design and construction. These structures include the lithological nature of the ground, structural features, and geological phenomena such as stratification, fracturing, fault zones, hydrogeological characteristics of the medium, and so on [1]. Therefore, it is necessary to exercise caution and conduct a tunnel stability study to reduce the damage caused by the different phenomena.

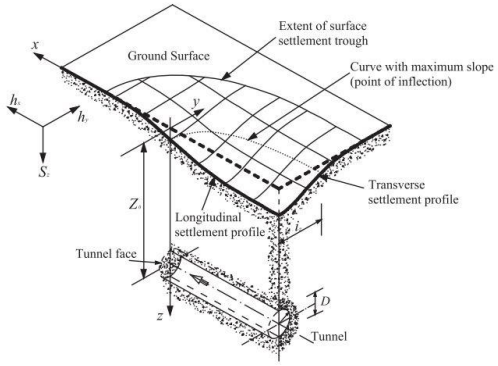

Fig. 1. Ground movements associated with tunnel construction [2].

Among analytical, experimental, and empirical methods, numerical simulation is a powerful and cost-effective tool for studying tunnel stability, selecting a suitable reinforcement strategy, and investigating the effect of various factors on it. In this regard, Mirsalari et al. (2017) proposed a finite difference/boundary element method (FD/BEM) to numerically measure the displacement, stresses, and horizontal strains for a conventional subsided area due to underground excavations [3]. Zhou et al. (2018) conducted a study on the interactions between rock and TBM under high stress and water pressure during the excavation of a deep tunnel by TBM using FLAC3D numerical software. They used a hydro-mechanical coupled model in FLAC3D to investigate rock mass deformation and pore pressure development. The numerical model results achieved by Zhou et al., 2018 can be used to determine the depth of influence of excavation on both deformation and pore pressure [4]. Hasanpour et al. (2017) investigated the jamming mechanism through a three-dimensional simulation of the TBM and ground using FLAC3D. They performed numerical simulations under different combinations of overburden and geological conditions. The authors stated that numerical simulation with FLAC3D software can be used to evaluate the effect of adverse geological environments on TBM. The simulations can also forecast the pressure on the shield and pre-estimate the required thrust force during excavation [1]. Recently, Abdollahi et al. (2019) accurately simulated the TBM motion in a faulty zone using FLAC3D and Phase2 software. The findings of their modeling indicated that the instability of the tunnel occurs in the Lalezar fault zone, which is one of the most challenging faults in the southern part of Iran, in Kerman province. To stabilize the tunnel during excavation, reinforcement operations must be taken into account. They simulated six stabilization operations and concluded that the combination of the umbrella arch method with the radial grouting method is the most appropriate scenario for the TBM to pass through the faulty zone [5]. Lui et al. (2022) used numerical simulation based on the discrete element method (DEM) - continuum mechanics coupling method to model the cutting of some existing bridge piles foundation along Line 12 of the Beijing Metro excavated by earth pressure balanced (EPB) shield machine. They stated that the effect of different parameters on the thrust force, displacement of the pile, and the torque of the EPB are in good agreement with the monitored data in the field and the theoretical method [6].

On the other hand, the behavior of the earth changes with stress redistribution due to tunneling. Therefore, more attention should be paid to the interaction between the soil, tunnels, and other underground infrastructures (gas, oil and water pipelines, power cables, etc.).

This stress redistribution is due to soil arching, as a transfer of load from mobilized parts of the soil to adjacent stationary parts [7-10]. In general, the soil arching phenomenon is divided into two different types active and passive. Active soil arching is a prominent phenomenon in geotechnical projects, such as retaining structures under active mode [11-15]. On the other hand, passive soil arching is prominent in geotechnical projects, such as undercut slopes, pile-reinforced slopes, retaining walls under passive mode, and tunnels [16-19].

One of the most common and controversial issues in this regard is ground settlement and its effect on buried pipelines due to tunnel excavation. Pipelines are prone to various forms of failure, including transverse fracture due to longitudinal pipeline bending, longitudinal split due to ring bending, and leakage at joints and service connections. Vorster, (2005) identified that transverse ground movements caused by tunneling, as shown in Fig. 2, are the primary concern for buried pipelines. He stated that tensile strain, joint rotation, and joint axial pullout were the predominant failure modes [20, 21].

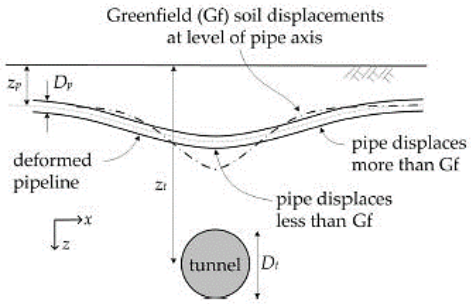

Fig. 2. The effects of tunneling on buried pipes [21].

The pipe experiences different loading due to tunnel construction. The loads and displacements that the pipeline experiences during tunnel construction depend on the relative properties of the pipe and soil. If the pipe is much stiffer than the soil (perfectly rigid case), it will carry the load of the soil above it and experience no bending. If the stiffness of the pipe is much less than that of the soil (infinitely flexible case), the soil and pipe will displace as if the pipe did not exist. Fig. 2 illustrates an intermediate state where the pipe bends to some extent due to ground displacement. This is the expected behavior of buried pipes, where the central part of the pipe (above the tunnel centerline) is displaced less than Greenfield, and the areas at the sides of the tunnel are displaced more than Greenfield [21].In recent decades, several kinds of research have been conducted on the interaction between tunnels, pipes, and soil. Vorster and Klar developed an analytical equation between soil, tunnel, and pipe interaction in 2005 [22]. In 2008, Klar et al. used numerical and analytical methods to study soil and pipeline interaction [23]. From 2009 to 2011, Marshall et al. investigated the interaction between soil, pipe, and tunnel using a centrifuge machine [24]. Between 2010 and 2011, Wang et al. developed Winkler's analytical equations with closed-form solutions and numerical modeling [25]. In 2015, Klar et al. proposed equations about the direction of the pipe and the tunnel axis using centrifugal modeling [26]. In 2016 Wang et al. measured ground and pipeline settlement by using centrifuge testing [27] and determined the limit of rotation angle in jointed pipelines [28]. Also in 2017, Ma et al. conducted physical modeling to investigate the impact of twin tunnels on pipeline displacement with centrifuge [29]. Shi and Zhang (2017) expanded Winkler's equation for clay [30]. Klar (2018) developed analytical equations using the Fourier series for pipeline and tunnel interaction [31]. Recently, Lin and Huang (2019) developed an analytical solution involving the Pasternak model to estimate the jointed pipeline's bending moment and deflection. Their studies showed that the distribution and number of joints have a mild effect on pipe deflection, while significantly affecting pipe bending moment. Furthermore, they discovered that pipe deflection is less sensitive to shear stiffness than pipe bending moment [32]. Saboya et al. (2020) conducted a study to investigate the mechanism of pipeline deformation under traffic load and the suitability of the modified Spangler-Iowa formula, coupled with the Boussinesq theory in predicting the deformation of pipelines. The authors used a geotechnical centrifuge physical model and numerical back-analysis using ABAQUS software. The results showed that the modified Spangler-Iowa formula together with the Boussinesq theory is somewhat conservative and the degree of conservatism increases with the embedment ratio [33]. Guan et al. (2020) numerically studied the effect of initiation charge, clear distance, and soil properties on stress response and velocity of square, circular, and horseshoe-shaped pipelines due to tunnel blasting using ANSYS/LS DYNA software. The authors found that the tensile stress and peak value of velocity on the circular pipe were the highest when the clear distance decreased and the initiation charge increased, followed by the square and the last was the horseshoe pipeline. They also stated that the peak tensile stress and the peak vibration velocity of the pipeline are the smallest when the pipeline is surrounded by clay and rammed sand, while pipes surrounded by pebble sand experience larger stress and peak vibration velocity [34]. Lin et al., (2020) proposed analytical solutions to forecast the response of the overlying soil and the pipeline. They found that gap formation beneath the pipeline reduces its bending moment and deflection created by tunneling. Furthermore, they discovered that pipelines with larger intersection angles concerning the tunnel alignment are predicted to withstand more bending moments [35]. Xia et al. (2021) conducted full-scale blasting experiments on a pipeline buried in a silty clay layer to analyze the impact of blasting vibration on adjacent reinforced concrete pipelines with gasketed bell-and-spigot joints. They measured the vibration velocity and dynamic strain variation of the pipe segments and joints subject to blasting vibration. Furthermore, they used LS-DYNA numerical software and field measuring data to compare the response of continuous and jointed pipes and determine the influence of pipe joints on the whole pipeline [36]. Yuan et al. (2022) utilized a unified three-dimensional upper-bound finite element method to investigate the support pressure assessment of tunnels around leaking pipelines. They examined the impact of groundwater level, water pressure, length of leakage, leaking location, and hydraulic

properties on tunnel stability. Additionally, they concluded that pipeline leakage can increase the limited support pressure of the tunnel. Moreover, they discovered a strong correlation between pore water pressure and the limit support pressure at the tunnel head [37]. Xia et al. (2023) investigated the behavior of cross-highway pipelines under rolling action of heavy vehicles, which can lead to pipeline damage. The authors established a numerical model by combining Adams and ABAQUS software to measure the pipeline's dynamic stress response and ultimate bearing capacity under vehicle load. The results presented that the stress on the pipeline is related to the vehicle diameter and load. The stress on the pipeline decreases with the increase in vehicle speed. When the burial depth of the pipeline reaches 1.5 m, the protective effect of soil on the pipeline is low. The authors also defined the overload warning index according to the Von Mises stress and established vehicle overload warning curves. On-site application showed that vehicle overload warning curves are exact and can provide guidelines for safe pipeline operation [38]. In recent years, researchers have focused on twin tunnel modeling [39] and pipelines overlapping.

Therefore, when excavating tunnels in urban areas, it is necessary to take into account the existence of various natural structures, geological phenomena, and service infrastructures such as gas, water, and wastewater pipelines to prevent possible hazards. These issues are quite complicated since they involve soil-structure interaction, therefore to prevent possible hazards, it is necessary to understand the behavior of the ground concerning tunnel convergence, the mechanism of soil-pipe interaction, the resistance properties and geometry of the pipe, tunneling-induced ground settlement, governing equations of soil-pipe settlement, the effects of tunnel depth, size, soil relative density, and volume loss on vertical and horizontal displacement, settlement, shear strain, dilation, pipe bending, and gap formation and the strain and stress components induced in the pipeline due to the displacement of the ground.

In this paper, the effects of various parameters influencing the tunneling-induced pipeline deformation, which have been examined by various researchers, are investigated. The results of different methods related to soil-pipe interaction are compared and discussed.

2. TUNNELING AND ITS EFFECT ON GROUND SETTLEMENT

Tunnel excavation causes convergence, and settlement, and changes the stress field around the tunnel. The ground settlement during tunneling depends on various factors such as medium type, tunnel depth, excavation method, and surcharge on the ground surface. Tunnels are usually excavated in residential areas where most surface structures are located near the tunnel and are affected by the ground settlement. To tunneling-induced movements in sands, many centrifuge and 1g tests have been performed to study the effects of tunnel depth, size, soil relative density, volume loss, and stratification [21, 40-47]. Also, empirical, semi-analytical, and analytical methods to evaluate ground movements and stress fields due to tunneling in sands have been developed by Franza and Marshall (2019) and Khandouzi and Khosravi (2023) [47-49]. Based on experimental tests, the most common shape for the ground settlement is a Gaussian curve. However, due to the surcharge on the ground surface, the shape of the settlement curve changes and does not follow the Gaussian curve. Also, by reducing the depth of the tunnel or decreasing the soil resistance above the tunnel, ground surface displacement increases. This displacement depends on many factors, such as excavation method, tunnel depth and geometry, and geological and geo-mechanical conditions. Peck (1969) [50] and O'Reilly & New (1982) [51] conducted the first investigations into this issue. Peck (1969) presented the ground settlement as follows:

$$s_v(x) = \frac{n}{n-1+\exp(\alpha \frac{x^2}{i^2})} s_{\max} \quad (1)$$

$$s_{\max} = \frac{v_{loss}}{i\sqrt{2\pi}} \quad (2)$$

$$n = \exp(\alpha).\frac{2\alpha - 1}{2\alpha + 1} + 1 \quad (3)$$

$$i = kz_0 \quad (4)$$

Where S_v(x) is the ground settlement at a horizontal distance of x from the tunnel axis, S_{max} is the maximum settlement, i is the inflection point of the ground settlement curve as shown in Fig. 3 according to Eq. (4), k is a dimensionless parameter depending on the type of soil, Z_0 is the depth of the tunnel, x is horizontal distance from tunnel axis, n is a shape function parameter controlling the width of the profile according to Eq. (3), V_{loss} is the soil volume loss, and α is a parameter depended on n. If n = 1, the ground settlement shape will reduce to the following Gaussian curve.

$$s_v(x) = s_{\max} exp(\frac{-x^2}{2i^2}) \quad (5)$$

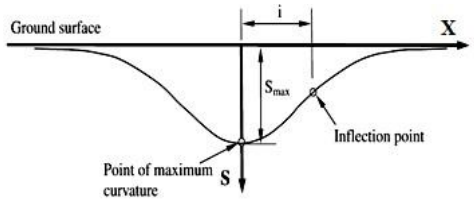

Fig. 3. Gaussian ground settlement profile induced by tunneling [52].

The ground settlement profile is a function of the soil grain size. For example, by changing the soil type from clay to sand, the soil grain size increases and α becomes higher, therefore the settlement profile becomes narrower. Many experimental equations have been suggested for the estimation of inflection points, some of them are presented in Eqs. (6-8).

$$i_1 = 0.386.z_0 + 2.84 \quad (6)$$

$$i_2 = 0.5.z_0 \quad (7)$$

$$i_3 = 1.392.(\frac{D}{2}).(\frac{Z_0}{D})^{0.704} \quad (8)$$

Where *i* is the inflection point of the ground settlement curve, Z_0 and *D* are the depth and diameter of the tunnel, respectively.

3. SOIL-PILE INTERACTION MECHANISMS

Fig. 4 illustrates the structural behavior of a buried pipeline affected by tunnel convergence. Vorster (2005) defined five mechanisms related to soil-pipe interaction: global greenfield soil settlement, gap formation below the pipe, positive down drag failure (when the pipe settles more than the soil), negative down drag failure (when the soil settles more than the pipe), and longitudinal interaction (shown by M-I to M-V in Fig. 4).

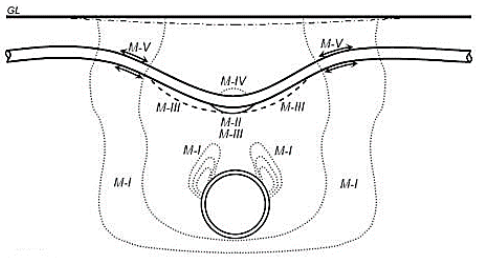

Fig. 4. Soil-pipeline interaction mechanisms behavior due to tunnel convergence [21].

Mechanism I is a global effect that increases soil strain resulting from tunnel convergence. Mechanisms II to V show local effects occurring adjacent to the pipeline. Mechanism II- gap formation, a gap occurs when the soil under the pipeline displaces more than the pipeline due to tunnel convergence [53-54], which means that the pipe at this location does not have any bearing support from the soil below it. Mechanism III, positive down drag, refers to a situation where the pipe settles more than the soil, which generally occurs near the tunnel centerline where a gap is formed. This event results in more pressure from the pipe on the soil in the area where mechanism III occurs. Mechanism IV refers to a situation where the soil settles more than the pipe, increasing the vertical load on the pipe. Mechanism V- longitudinal interaction, is related to the situation where the horizontal soil strain causes the load transferred to the pipe. The horizontal strain causes an additional tensile strain in the pipe, which can lead to tensile failure or joint pullout [20].

4. TUNNELING AND ITS EFFECT ON PIPELINE SETTLEMENT

The soil-pipe behavior mechanism, field observations, and experimental tests have proven that tunneling-induced ground settlement above the pipe differs from greenfield settlement. Therefore, under these conditions, modifying the governing equations of the soil-pipe settlement is necessary [29, 54-55].

Winkler (1867) developed the first and the most prevalent analytical solution available in the literature to investigate this principle by considering the soil around the pipeline as separate springs, as shown in Fig. 5. He studied how the pipeline interacts with the soil [56].

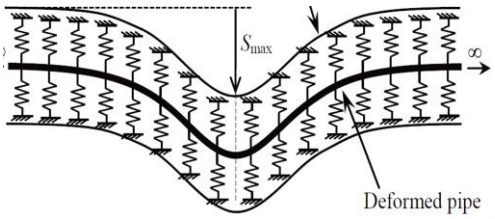

Fig. 5. Soil and pipeline interaction in the Winkler model [22].

Attewell et al. (1986) using the Winkler model (1867) with the subgrade modulus proposed by Vesic (1961), comprehensively investigated the soil-pipeline interaction. Klar (1986) developed Winkler's model (1867) based on the closed-form solution. In this solution, a new subgrade modulus (k) was presented instead of Vesice's subgrade modulus [22]. Klar (1986) explained that the force on the pipeline due to the tunnel excavation is a coefficient of the ground settlement, as follows.

$$F(x) = kS(x) \quad (9)$$

In this equation F(x) is the force on the pipeline, k is the subgrade modulus and S(x) is the ground settlement at a horizontal distance of x from the

tunnel axis. The force distribution on the pipeline, according to Eq. (9), is shown in Fig. 6.

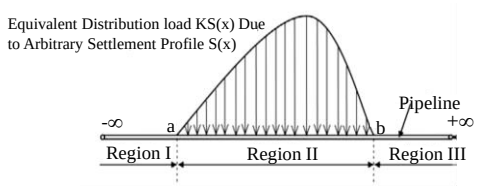

Fig. 6. The force distribution on the pipeline due to ground settlement [52].

Klar et al., 2005 compared closed-form Winkler solutions with the Vesic subgrade modulus and elastic continuum solution. They also suggested dimensionless charts that can estimate the maximum settlement and inflection point offset as well as used for any subsurface Gaussian settlement trough [57]. Klar et al. (2007) proposed a solution that applied a boundary integral formulation to describe the elastic continuum. A limiting force is incorporated to reflect relative pullout failure [58]. Klar et al. (2008) formulated analytical solutions for jointed pipelines by modeling the joints as rational springs to take account of their influence [23]. Based on a closed-form solution and numerical modeling, Wang et al. (2011) found that the deformation of the pipeline does not correspond to the soil. Despite the downward bending of the pipe, at some points, its movement is upward. Therefore, Wang et al. (2011) presented different subgrade moduli for upward bending (K_u) and downward bending (K_d) instead of Klar's subgrade modulus [25]. Those subgrade moduli can be obtained from the following equations [59].

$$k_u = \frac{q_u}{\delta_{ru}} \tag{10}$$

$$k_d = \frac{q_d}{\delta_{rd}} \tag{11}$$

$$q_u = N_\gamma \gamma H D \tag{12}$$

$$q_d = N_q \gamma H D + 0.5 \gamma N_\gamma D^2 \tag{13}$$

Where, k_u and k_d are the subgrade moduli of the soil in the bend up and bend down state, respectively. q_u and q_d are the soil resistance according to Eq. (12) and Eq.(13) in the bend up and bend down state, respectively, δ_{ru} and δ_{rd} are the pipe-soil relative displacement in the bend up and bend down state, respectively, D is the pipe diameter, H is the pipe depth and γ is the soil unit weight. N_γ and N_q are bearing capacity factors, which are functions of soil internal friction and can be obtained from Table 1 [60].

Table 1. Bearing capacity factors based on soil friction angle [60]

φ	N_q	N_γ
0	1	0
5	1.57	0.45
10	2.97	1.22
15	3.94	2.65
20	6.4	5.39
25	10.66	10.88
30	18.4	22.4
35	33.3	48.03
40	64.2	109.41

The effect of tunneling on the pipeline is usually studied by the changes in pipe-soil hardness and bending ratio. The pipe-soil hardness and pipe-soil bending ratio are obtainable from Eq. (14) and Eq. (15), respectively.

$$x = \frac{E_p I_p}{k_u^{0.9} k_d^{0.1} i^4} \sqrt{\frac{S_{max}}{i}} \tag{14}$$

$$y = \frac{\kappa_{p\max}}{\kappa_{g\max}} \tag{15}$$

$$\kappa_{p\max} = \frac{M_{\max}}{E_p I_p} \tag{16}$$

$$\kappa_{g\max} = \frac{S_{\max}}{i^2} \tag{17}$$

$$M_{max} = 0.6(kr_0)^{0.75} E_p I_p^{0.25} V_{loss} \tag{18}$$

Where x and y are pipe-soil hardness and pipe-soil bending ratio, E_p and I_p are the young modulus and the moment of inertia of the pipe, S_{max} is the maximum settlement, k_u and k_d are the subgrade moduli of the soil in the bend up and bend down state, respectively, i is the inflection point of the ground settlement curve, r_0 is the radius of the pipe, k_{pmax} and k_{gmax} are the subgrade modulus calculated according to Eq (16) and Eq.(17) respectively. V_{loss} is the soil volume loss, M_{max} is maximum bending according to Eq.(18). The diagram of the pipe-soil bending ratio versus the pipe-soil hardness, obtained from the numerical modeling of Shi et al. (2017) is shown in Fig. 7.

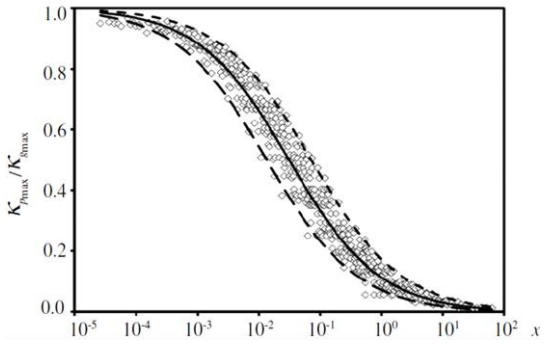

Fig. 7. The diagram of the pipe-soil bending ratio versus the pipe-soil hardness [30].

According to Fig. 7, when the pipe-soil hardness increases, the pipe-soil bending ratio decreases. Based on the numerical modeling, the relationship between the pipe-soil bending ratio (y) and the pipe-soil hardness (x) is obtained from the best-fit curve:

$$y = \frac{1}{7.72x^{0.59}+1} \tag{19}$$

The modified Winkler's solution based on the elastic method was done by Klar et al. in 2005 [57]. In their solution, they presented the equations of the bending moment for the pipe and ground using the continuous solution with the definition of the new subgrade modulus according to Eq. (20).

$$k = \frac{12E_s r_0}{i} \tag{20}$$

Where k is the subgrade modulus, E_s is the young modulus of soil, r_0 is the radius of the pipe and i is the distance from the tunnel centerline to the inflection point of the settlement trough.

Klar and Marshall (2015) studied the tunnel-pipeline interaction problem using an elastic-continuum approach and in their solution, the pipeline was assumed as an Euler-Bernoulli beam. They also demonstrated the principle of volume loss equality between the input greenfield settlement and the generated pipeline deflection [61]. Based on numerical simulation of the pipeline, Klar and Marshall 2015 also found that the pipeline settlement profile follows a Gaussian curve, similar to the soil settlement profile [61]. Hence, the pipeline has a settlement profile similar to the soil, as shown in Eq. (21).

$$u(x) = u_{max} exp(\frac{-x^2}{2i_p^2}) \tag{21}$$

Where U_{max} is the maximum vertical displacement of the pipe, i_p is the inflection point of the pipe settlement curve and x is the horizontal distance from the tunnel axis. Despite the same displacement curve shape for soil and pipe, due to their different resistance bending, their deformation is different. The resistance of soil and pipe to bending is checked with two parameters of the settlement coefficient (β) and the pipe-soil hardness factor (R). These two parameters are determined by Eqs. (22-23). The settlement coefficient (β) as a function of the pipe-soil hardness factor (R) is shown in Fig. 8.

$$\beta = \frac{i^2}{2i_p^2} \tag{22}$$

$$R = \frac{E_p I_p}{E_s i^3 r_0} \tag{23}$$

β is settlement coefficient, R is the pipe-soil hardness factor, i is the distance from the tunnel centerline to the inflection point of the settlement trough, i_p is the distance from the tunnel centerline to the inflection point of the pipeline settlement trough, E_p and I_p are the young modulus and the moment of inertia of the pipe respectively, E_s is the young modulus of soil, r_0 is the radius of the pipe. According to Fig. 8, when the pipe-soil hardness factor increases, the settlement coefficient decreases. On the other hand, the pipe-soil hardness factor has an inverse relation to its bending ratio. This variation has been shown in Fig. 9. In addition, the maximum pipe-soil bending ratio has a non-linear direct relation to the maximum displacement ratio of pipe and soil. This variation is shown in Eq. (24) and plotted in Fig. 10.

$$\frac{u_{max}}{S_{max}} = 1 + 0.3(\frac{M_{max}}{M_{max,gf}})^{0.115} \ln(\frac{M_{max}}{M_{max,gf}}) \tag{24}$$

$$\frac{M_{\max}}{M_{\max,gf}} = \frac{1}{1+1.1\frac{\alpha}{n} f_i (f_d R)^{2/3}} \tag{25}$$

$$f_d = \frac{1+0.93\frac{z_p}{r_0}}{1.07\frac{z_p}{r_0}} \tag{26}$$

$$f_i = \frac{2.18}{\sqrt[3]{\frac{i}{r_0}}} \tag{27}$$

Where, M_{max} and $M_{max,gf}$ are the maximum bending of the pipe and the soil, respectively. R is the pipe-soil hardness factor, n is a shape function parameter controlling the width of the profile and α is a parameter dependent on n, f_d and f_i defined according to Eq. (26) and Eq.(27). z_p is the depth of the pipe and r_0 is the pipe radius, i is the distance from the tunnel centerline to the inflection point

of the settlement trough, S_{max} and U_{max} are the maximum settlement and displacement respectively.

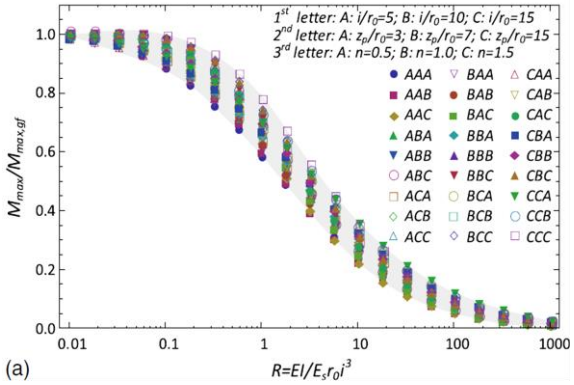

Fig. 9. The variation of the maximum pipe-soil bending ratio versus the pipe-soil hardness factor [26]

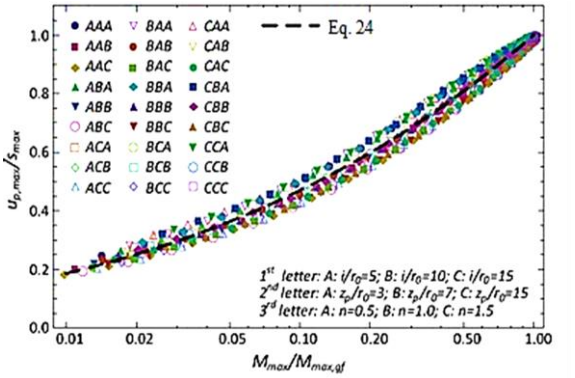

Fig. 10. The maximum displacement ratio of pipe and soil versus the maximum pipe-soil bending ratio [26].

Additionally, Klar et al. (2016) offered a design-oriented approach to evaluate the effect of tunneling on pipelines. Soil nonlinearity was assumed by iteratively calculating the equivalent stiffness in their solution [26].

5. PHYSICAL MODELING

The behavior of pipe above the tunnel due to convergence is difficult to observe in the field, as it occurs over long periods of time and requires costly and time-consuming data collection. Therefore, small-scale physical modeling can be used to investigate the pipe-soil interaction behavior above the tunnel. Experimental tests in geotechnical engineering such as retaining walls, foundations, undercut slopes, shafts, piles, pipeline, and tunnels are typically conducted under 1g conditions [62-68]. Over the past decade, numerous studies have employed centrifugal physical modeling and advanced image processing to investigate the stress and strain distribution in soil [69-72]. However, Physical modeling causes scale errors in experimental measurements. On the other hand, the behavior of geotechnical structures depends on the stress value, so they show different behaviors due to different stress levels. Therefore, the effect of stress-dependent behavior, besides the scale effect, causes a large error in physical modeling. The geotechnical centrifuge is a device that compensates for the stress level created by the scale effect. This issue is compensated by increasing the acceleration of gravity in the centrifuge and reducing the physical modeling errors.

Jacob and Vorster's modeling in 2002 and 2005 was the first centrifuge modeling in the field of soil-pipe interaction due to tunneling [61]. Marshall and his research team investigated the influence of tunneling on pipelines and piles [21, 73, 74]. More investigations were done by Zhou (2014) and Frabza (2016) to study the effects of tunnel depth, tunnel size, soil relative density, volume loss, and stratification [41, 42].

The centrifuge used by Marshall's research team had dimensions of 770*138*312 mm. The front side of the centrifuge had a low-friction Perspex glass. Marshall investigated surface and subsurface vertical displacements due to convergence by PIV, LVDT, and laser. The comparison is shown in Figs. 11 and 12 for normal and Perspex glass respectively.

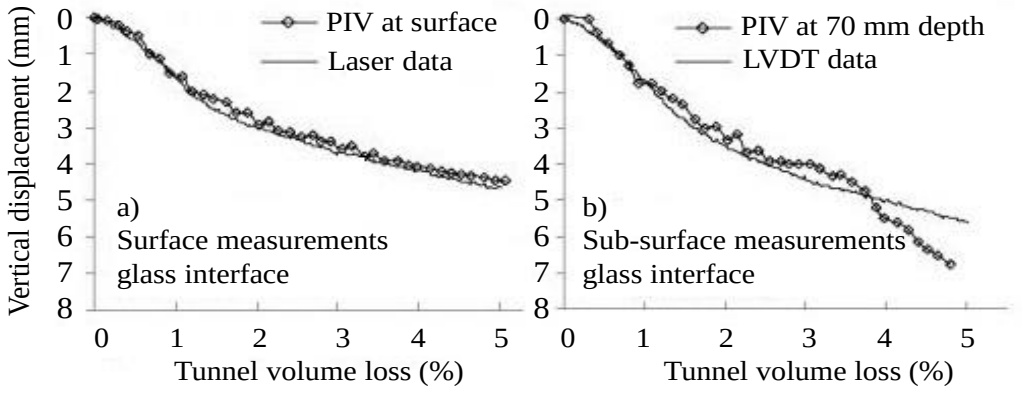

Fig. 11. Diagram of vertical displacement and tunnel volume loss for normal glass [74].

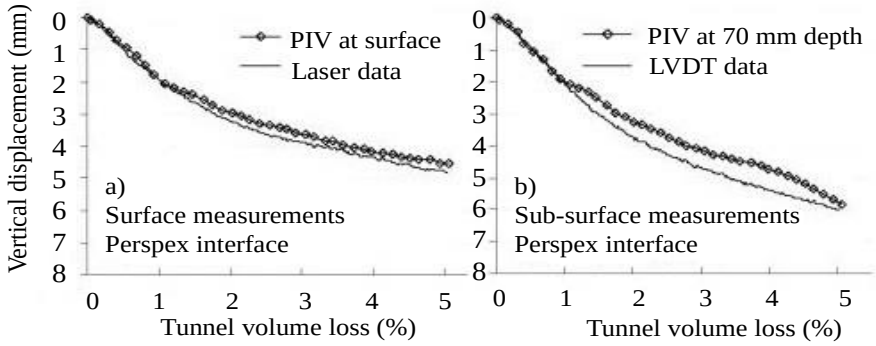

Fig. 12. Diagram of vertical displacement and the tunnel volume loss for Perspex glass [74]

Glass is often used as an interface material between the soil and the front wall because it has higher hardness than Perspex and prevents sand grains from scraping into the wall under high-stress levels (a phenomenon which causes increased boundary friction and affected the PIV measurements). Figs. 11 and 12 show a comparison between the PIV data and the surface (laser) and sub-surface (LVDT) data for both glass and Perspex. The PIV data agrees well with the measurements. However, glass causes optical problems that reduce the quality of the PIV analysis. Therefore, Perspex is preferred for the experiments since it does not significantly affect the PIV displacement data.

Fig. 13 illustrates the measurement of soil volume loss at different depths. Near the tunnel crown at the beginning of the excavation, the soil volume loss is equal to the tunnel volume loss. When the tunnel convergence increases, the volume loss increases with a low gradient and then decreases. Similar behavior is observed for the soil near the surface as well. The results of the two tests differ from each other due to the friction effect. If the friction between the centrifuge box and the soil is zero, a more realistic model can be obtained with more reasonable results.

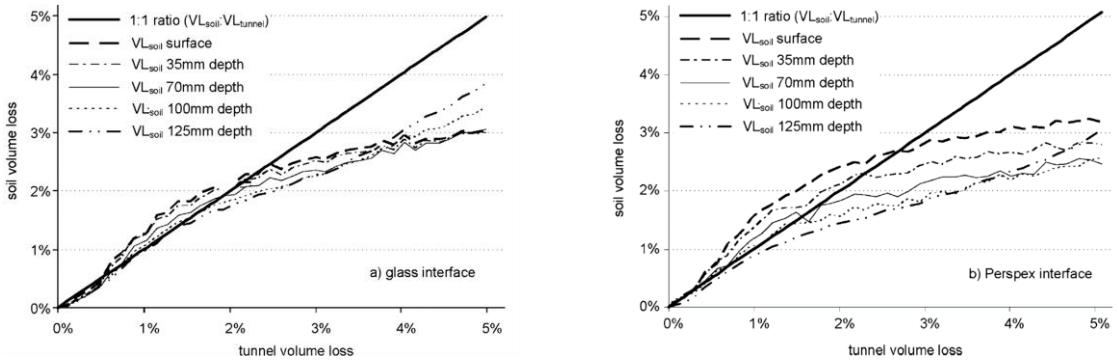

Fig. 13. The soil volume loss changes with the tunnel volume loss for ordinary glass and Perspex [74].

After comparing Figs. 11, 12, and 13, it can be concluded that the PIV method for displacement measurement in Perspex is superior to that in normal glass. This is due to the high friction between ordinary glass and soil, the reduced quality of photography, and the poor performance of ordinary glasses in reflecting light.

Due to the acceptable results of the PIV method in Perspex, Marshall used this method to measure pipe and soil displacement (vertical and horizontal displacement), settlement, shear strain, dilation, pipe bending, and gap formation using centrifuge tests. Fig. 14 shows the setup for these tests, where A is the tunnel model, B is the PIV, C is the laser, D is the LVDT and E is the pipe. Marshall et al. (2010) investigated the vertical and horizontal displacement and settlement of different pipes (rigid, intermediate, and flexible pipe according to Table 2) and compared their results.

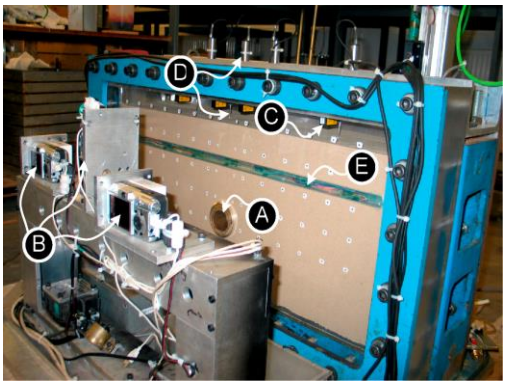

Fig. 14. A view of centrifuge box [74].

Table2. Mechanical and dimensional properties of Marshall et al. (2010) centrifuge modeling pipes [24]

pipe	Material and young's modulus	Cross section (mm)	EI² (Nm²)
Rigid	Aluminum, E=70 GPa	Square, w=19.05,t=1.63	809.6
Intermediate	Aluminum, E=70 GPa	Circular, r=9.53, t=1.63	238.5
flexible	Perspex, E=2.9 GPa	Circular, r=8, t=2	6.44

Based on the results of the centrifuge test, Marshall (2009) concluded that at small convergences, the magnitudes of vertical and horizontal displacements are similar for all pipe tests, and are relatively uniform throughout the depth of soil in the chimney zone. However, when the tunnel convergence increases by more than 1%, it causes a discontinuity in the displacement field, as shown in Figs. 15 and 16.

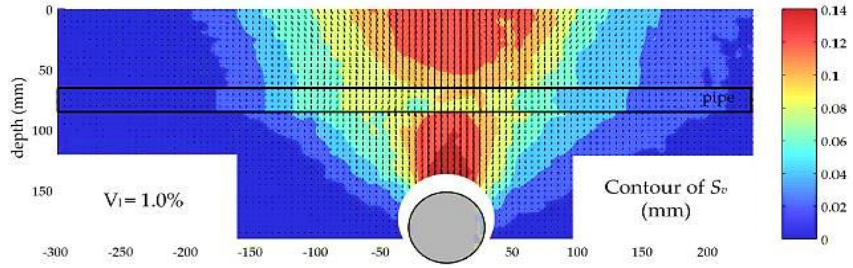

Fig. 15. A sample of vertical displacement contour for centrifuge test [21].

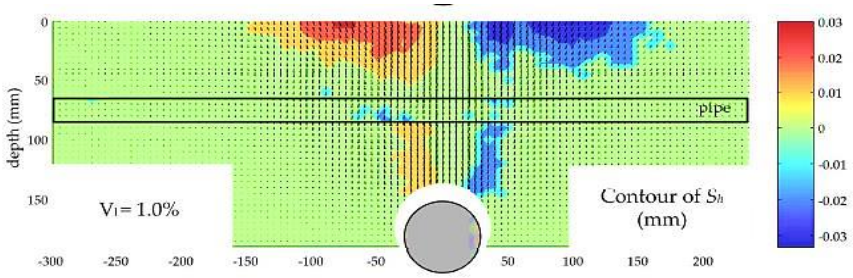

Fig. 16. A sample of horizontal displacement contour for centrifuge test [21].

Figs. 17 and 18 show that the settlement of the soil and pipe tests are different. The pipe rigidity creates a resistance force against the ground settlement, causing the pipe test to settle less than the soil. The displacements occurred in the pipe and the soil near the tunnel crown is higher than the ground surface.

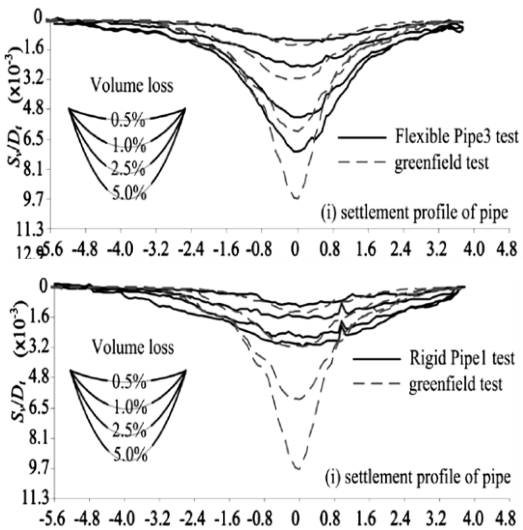

Fig. 17. Rigid and flexible pipeline settlement (measurement at the pipe level) [24].

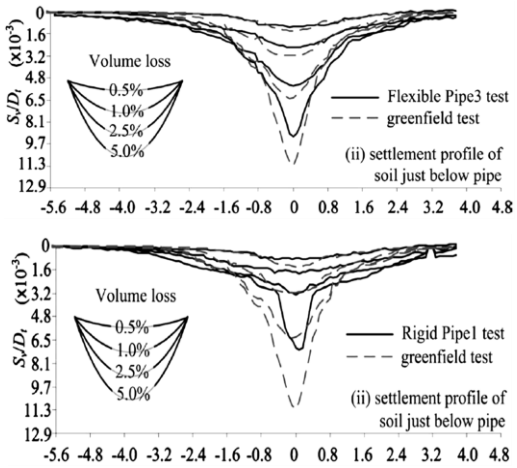

Fig. 18. Rigid and flexible pipeline settlement (measurement under the pip) [24].

Figs. 15-18 show that the presence of the pipe causes a change in the amount of displacement and the stress and shear strain field in the soil environment. To investigate the effect of the pipe on the shear strain field, a comparison has been made between the test results according to Fig. 19. The shear strain values, shown in this figure, are calculated according to Eq. (28).

$$\gamma = \sqrt{(\varepsilon_{xx} - \varepsilon_{zz})^2 + 4\varepsilon_{xz}^2} \qquad (28)$$

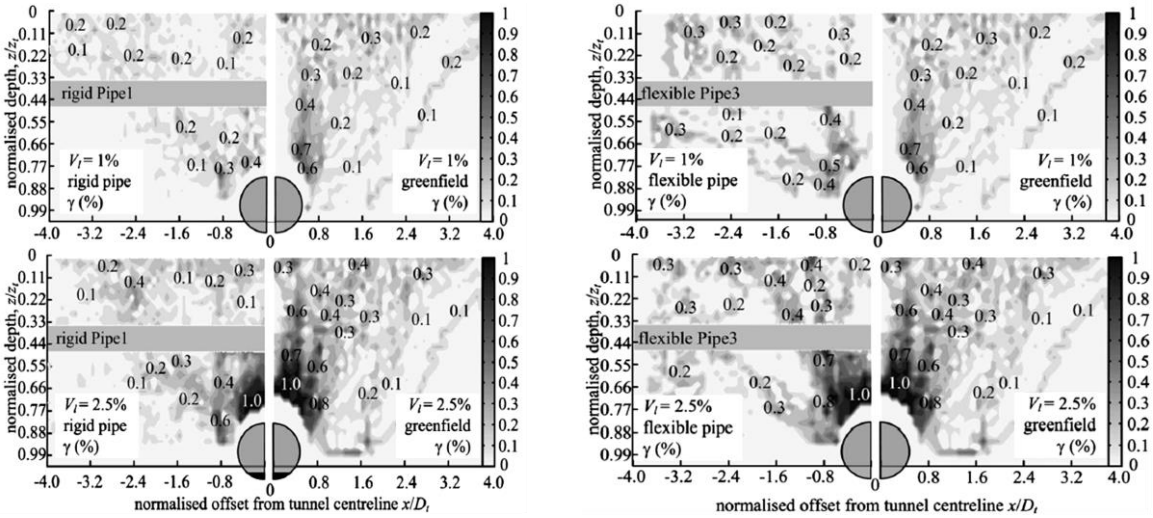

Fig. 19. The influence of pipe rigidity on the shear strain contours around the tunnel [24].

According to Fig. 19, the shear strain near the tunnel crown is higher than the ground surface and an increase in the tunnel volume loss lead to an increase in shear strains. In addition, the maximum shear strain for a flexible pipe is higher than that of a rigid pipe. This phenomenon occurs due to the settlement of flexible pipes. By experimentally measuring pipe settlement and bending, it is possible to choose a suitable pipe according to the tunnel diameter, convergence, and depth. The experimental results indicate that the dilation angle in the contraction zone ranged from -20 to 0 degrees, while in the expansion zone, it ranged from 0 to 10 degrees, and in some areas, it was as high as 20 degrees. A comparison between the dilation angle measured in centrifugal tests and the shear strain has shown a good agreement between the dilation angle value and the shear strain.

Table 3 displays the soil and pipe settlement and the shape function of different types of pipes. According to the table, as the tunnel volume loss increased, the vertical displacement of the ground and pipe increased while the inflection point (i) and the function parameter of the Gaussian curve (α) decreased. These changes indicate that as the tunnel volume loss increased, the ground and pipe settlement profile became wider.

Table 3. Soil settlement parameters and types of pipes obtained from centrifuge modeling [24]

$V_{loss\ (\%)}$	S_{max} (mm)				i (mm)				a			
	GF	P1	P2	P3	GF	P1	P2	P3	GF	P1	P2	P3
0.5	0.07	0.06	0.05	0.07	55	96	72	54	0.17	0.38	0.28	0.11
1	0.16	0.1	0.1	0.15	51	99	72	54	0.12	0.37	0.27	0.11
2.5	0.35	0.17	0.18	0.33	39	102	72	52	0.04	0.33	0.26	0.1
5	0.65	0.19	0.22	0.44	24	100	71	50	0.01	0.29	0.25	0.1
Note: GF: Ground surface, P1: pipe1, P2: pipe2, P3: pipe3												

Centrifuge testing indicates that pipe bending occurs when tunnel volume loss increases. The pipe bending can be positive or negative. Positive bending (downward) occurs near the tunnel axis, which is marked by sagging, but negative bending (upward) occurs at a distance from the tunnel axis, which is known as hogging. Fig. 20 shows the maximum value of bending due to tunnel volume loss.

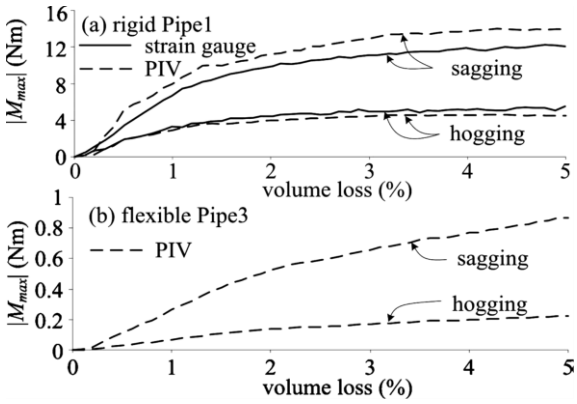

Fig. 20. The absolute maximum bending occurred in the pipes based on the tunnel volume loss [24].

Based on Fig. 20, the comparison between the results of the strain gauge and PIV methods indicates good agreement between the two methods. Due to the cost and difficulty of using a strain gauges, the PIV method can be used to estimate pipe bending. Additionally, Fig. 21 shows a comparison between PIV and numerical modeling that the physical and numerical modeling results are compatible when the tunnel convergence increases.

To compare the amount of bending that occurred in the pipes and the ground, the profile of the bending is shown in Fig. 22.

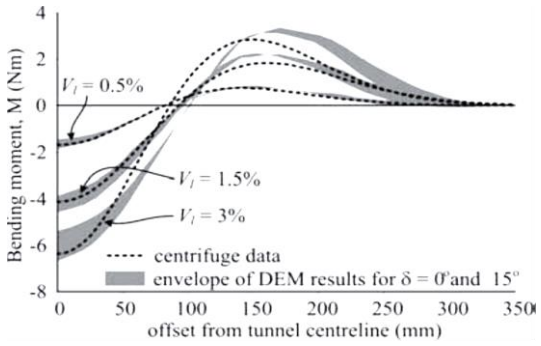

Fig. 21. Comparison between physical and numerical modeling for the developed bending moment in pipes[73].

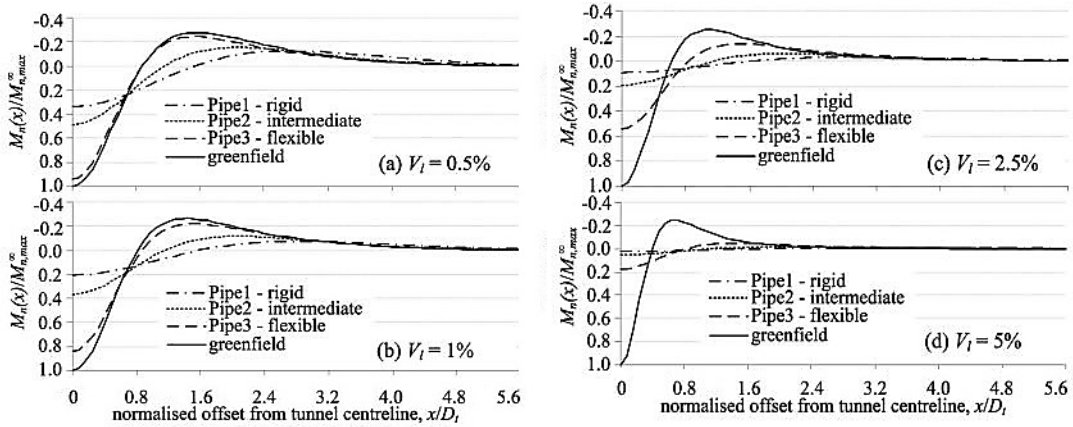

Fig. 22. Comparison between the amount of bending that occurred in the pipes and the ground [24].

In Fig. 22, the negative value of the vertical axis indicates hogging and the positive value indicates sagging or downward bending. When the tunnel volume loss is low, the minimum bending occurs in the rigid pipe, and the maximum bending occurs in the flexible pipe. Additionally, the flexible, medium, and rigid pipes experience the most changes in bending force acting on them, respectively.

Tunneling can cause gap formation beneath pipelines, which can affect their bending behavior and loading conditions. Fig. 23 compares the displacement of pipelines and soil for three types of pipes (rigid, intermediate, and flexible) as tunnel convergence increases. The Fig. 23 (d) also shows the changes in gap height with tunnel convergence for each pipe type. Flexible and intermediate pipes exhibit gap initiation at 0.5 to 1% tunnel convergence, while rigid pipes do not show gap formation until 3.5% convergence. After convergence reaches 4.5%, the rate of increase in gap height is similar for all pipe types [21].

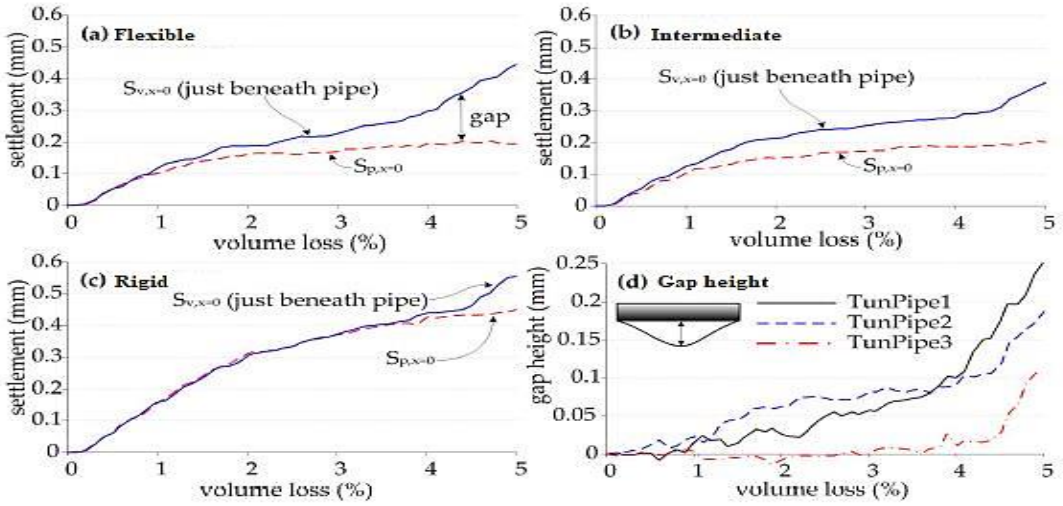

Fig. 23. Evaluation of gap formation beneath pipeline [21].

Klar et al. (2015) [26] used a comprehensive method to design the pipe near the tunnel. This method involved using closed-form, numerical, and experimental results. They used several pipes with different depths and diameters in both centrifuge and numerical methods. The maximum bending of the two methods was compared with the analytical method. Table 4 shows the dimensions and bending stiffness (EI) of pipes for a tunnel with D=4.65m and Z=13.65m.

Table 4. The dimension and bending stiffness (EI) of the pipes [26]

Test	D_p (m)	Z_p (m)	EI (kN.m^2)
CenTunPipe1	1.43	5.55	25.62*10^6
CenTunPipe2	1.43	5.25	7.55*10^6
CenTunPipe3	1.2	5.4	0.2*10^6
DEMTunPipe1	1.43	5.63	7.55*10^6
DEMTunPipe2	1.8	2.73	8*10^6
DEMTunPipe3	2.3	5.63	25.75*10^6
DEMTunPipe4	1.8	5.63	0.2*10^6
DEMTunPipe5	2.3	2.73	25.75*10^6
DEMTunPipe6	1.8	2.73	0.2*10^6
Note: D_t=4.65 m, Z_t=13.65 m			

The comparison of the close-form solution, the experimental, and numerical method results have been shown in Fig. 24.

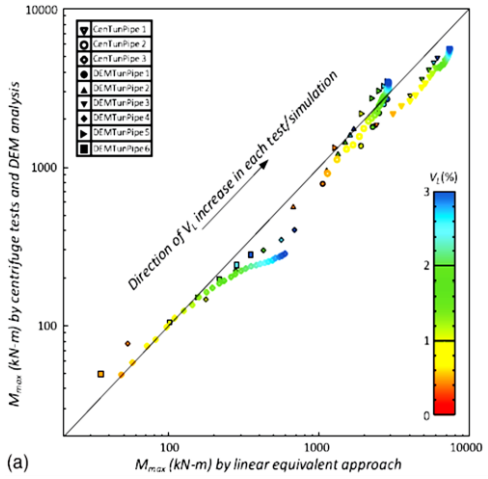

Fig. 24. Comparison of bending results on pipes in numerical method and centrifuge modeling with elastic solution [26].

Points close to the middle line of the diagram indicate correspondence between the numerical, experimental, and closed-form solutions. According to Fig. 24, the accuracy of results obtained from the closed-form solution for deep flexible pipes decreases with an increase in tunnel volume loss. Fig. 25 shows changes in the maximum bending ratio with tunnel volume loss. According to this figure, the rate of maximum bending in the soil is higher than in the pipe when tunnel volume loss increases. An important parameter in Fig. 25 is the interaction reduction index (IRI), which is obtained from Eq. (29).

$$IRI = 1 - \frac{M_{\max}}{M_{g,f\ \max}} \tag{29}$$

Where, M_{max} and $M_{gfmax,}$ are the maximum bending of the pipe and the soil, respectively. This index shows the degree of interaction between the soil and the pipe, and its value can range from 0 to 1. A coefficient value of 1 indicates that minimum bending occurred in the pipe, while a coefficient value of 0 indicates a very close interaction between the soil and the pipe. According to Fig. 25, the ratio of pipe to soil bending is close to 1 for flexible pipes, while this ratio is close to 0 for rigid pipes.

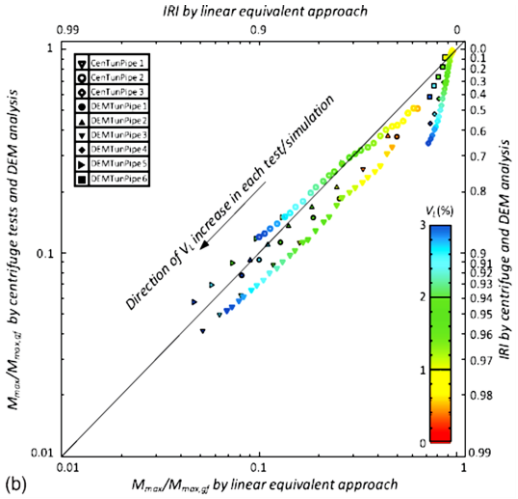

Fig. 25. Comparison of bending ratio results in numerical method and centrifuge modeling with elastic solution [26].

So far, all physical modeling research has investigated the behavior of pipelines and the ground near the tunnel crown in two dimensions, with the pipe placed at a 90-degree angle to the tunnel axis. Wang et al. (2016) [27] investigated the three-dimensional behavior of pipelines near the tunnel crown when placed at 90 and 60-degree angles to the tunnel axis. The dimensions of the box, tunnel, and pipe are shown in Fig. 26.

In this modeling, displacements were measured using strain gauges and LVDTs. The dimensions and mechanical properties of the soil and pipes were similar in both tests for comparison purposes. The amount of soil settlement at different distances from the tunnel axis was measured at each stage of tunnel convergence. The settlement profile is shown in Fig. 27.

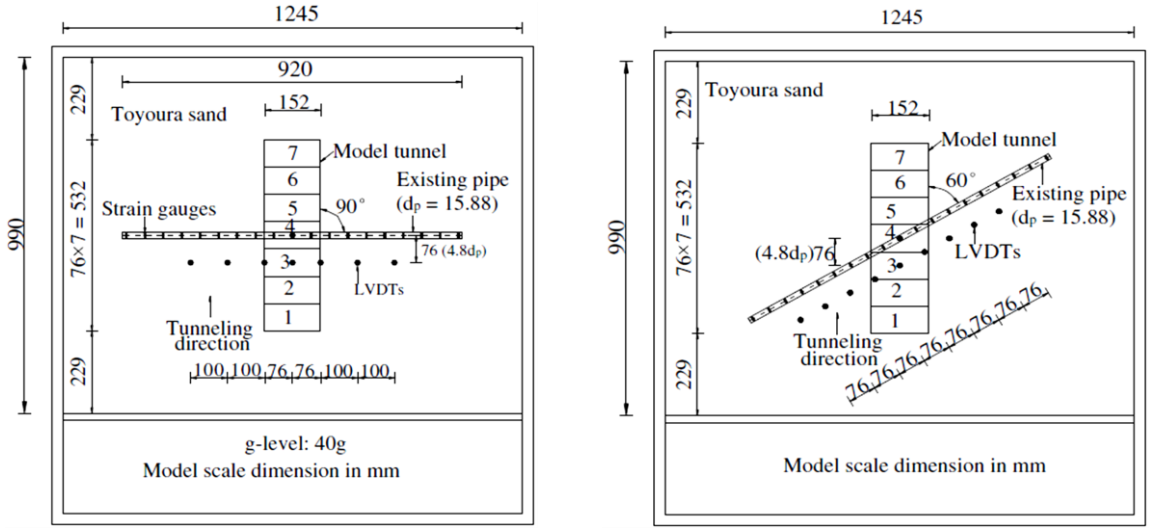

Fig. 26. A cross-section of the centrifuge modeling with the pipe direction 60 degrees and perpendicular to the tunnel [27].

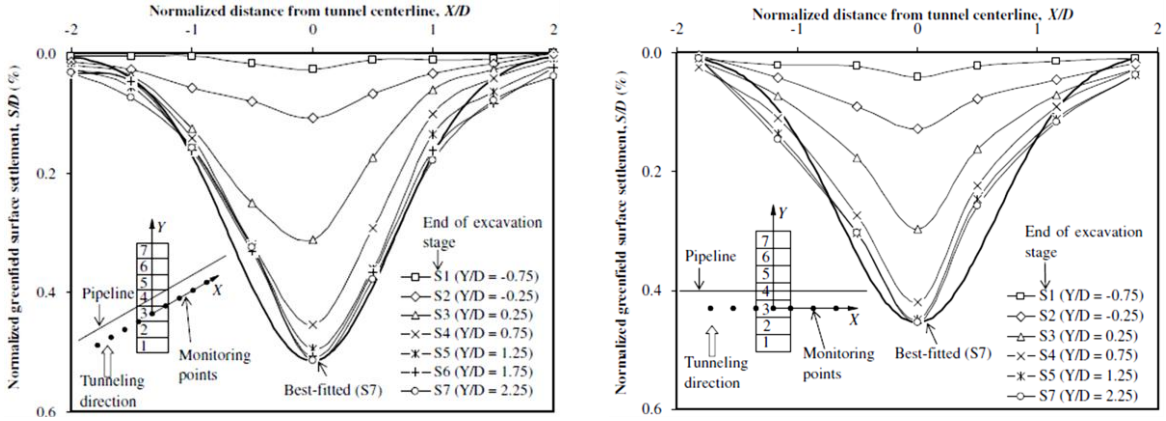

Fig. 27. Ground settlement profile at different stages of excavation with the direction of the pipe at 60 degrees and perpendicular to the tunnel axis [27].

According to Fig. 27, in the first test where the pipe was placed perpendicular to the tunnel axis, the maximum soil settlement (27.4 mm) occurred above the tunnel axis and decreased to 0.04% of the tunnel diameter (2.4 mm) at a distance of 1.8 D from the tunnel axis. In the second test (pipe with an angle of 60 degrees to the tunnel axis), the maximum soil settlement occurred above the tunnel axis and was 0.51% of the tunnel diameter (31 mm) in size. In both tests, 95% of soil settlement occurred between 1.25 and -1.25 times the tunnel diameter from the tunnel axis, and 75% of soil settlement occurred between 0.75 and -0.75 times the tunnel diameter.

Studies conducted recently are typically focused on a specific aspect of the subject and serve a particular purpose. Recently, Aljaberi et al. (2024) used large-scale experimental tests to study the behavior of buried flexible high-density polyethylene (HDPE) pipes, in sandy soil with and without voids subjected to cyclic loading. The large-scale fully instruments laboratory testing setup has been shown in Fig. 28 [75].

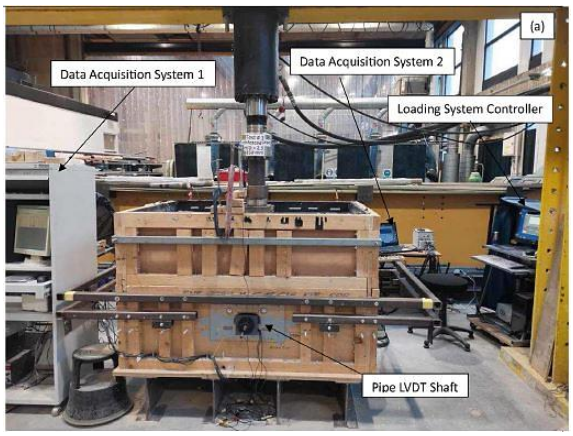

Fig. 28. The large-scale fully instruments laboratory testing setup [75].

The testing program and the value of applied cyclic loading phases presented in Table 5. The crown and invert of pipe deformation or settlement showed in Fig. 29 against the number of cycles under variation of H/D (soil height per pipe diameter) with and without void presences.

Table 5. The testing program and the value of applied cyclic loading phases [75]

Test series	Test type	Tests	Test configuration (H/D)	Load Phase	Number of cycles	Mean Load (kN)
B	Without void presence	T3	1.5	Phase 1	3000	15
		T4	2	Phase 2	1000	20
		T5	2.5	Phase 3	1000	25
C	With void presence	T6	1.5	Phase 1	3000	15
		T7	2	Phase 2	1000	20
		T8	2.5	Phase 3	1000	25

Fig. 29 showed that the pipe with void presence at the spring-line experienced higher deformations at its crown and invert, compared to the case of buried pipes without void presence. This is due to the existence of voids leading to uneven distribution of loads around the buried pipe. Also, increasing the pipe burial depth (with and without voids) would reduce pipe deformation. This is because the increased soil volume interacts with the stresses transferred to the pipe, resulting in load mitigation on the pipe and decreasing deformation [75].

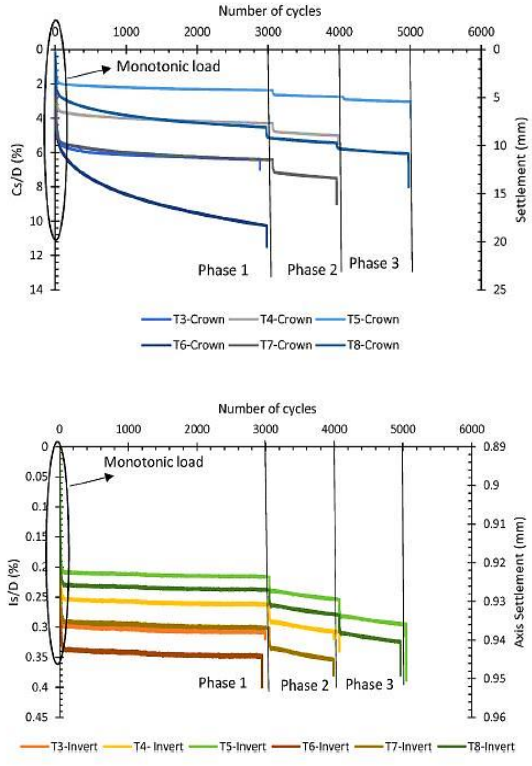

Fig. 29. Crown and invert deformation versus number of cycles [75].

Fig. 29 indicates that for buried pipes without void presence, most of the crown and invert settlement occurred in the first 30 cycles, regardless of the pipe's burial depth. In contrast, most of the invert and crown deformation or settlements happened after a considerable number of loading cycles, for buried pipes with void presence [75].

6. GROUND AND PIPELINE SETTLEMENT DUE TO TWIN TUNNELING

With the progress of public transportation and the subway, the construction of the twin urban tunnels in the vicinity of facilities and buildings is becoming increasingly common. Therefore, it is necessary to investigate the impact of twin tunnels on facilities and pipes. In 2021, some researches were conducted regarding twin tunnels and their effect on ground settlement and the deformation of adjacent pipes. This section involved a 3D modeling of a real example of twin tunnels according to Fig. 30.

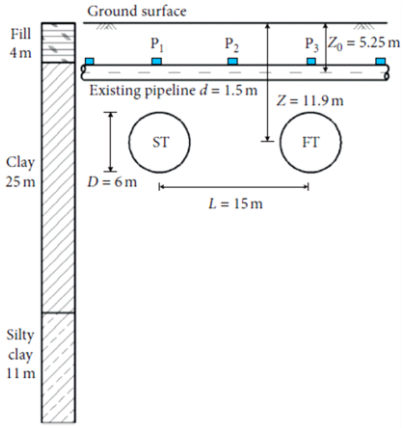

Fig. 30. Profile of a twin-tunnel passing under an existing pipeline [39].

The settlement profile of the ground and existing pipeline, caused by twin tunnels, is a W-shaped profile obtainable from the following equation [39].

$$S = S_{max,s}.\exp[\frac{(x-0.5L)^2}{2i_s^2}] + S_{max,f}.\exp[\frac{(x+0.5L)^2}{2i_f^2}] \quad (30)$$

Where, L is the distance between two tunnels, i_f and i_s are the inflection point of the settlement profile caused by the first and second tunnel, respectively and $S_{max.s}$ and $S_{max,f}$ are maximum

settlement caused by the first and second tunnel, respectively. A comparison between ground settlement and pipeline displacement with prototype measurements and numerical simulation during the construction of the first and second tunnels is shown in Fig. 31. In the numerical simulation, the first tunnel was excavated, followed by the excavation of the second tunnel.

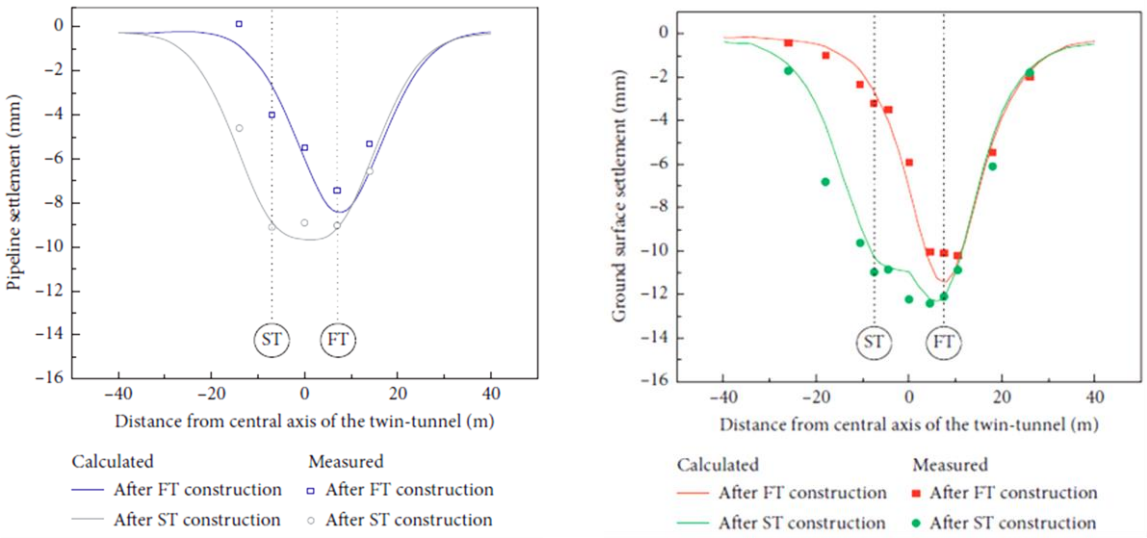

Fig. 31. Comparison of calculated and measured settlement of ground surface and pipeline [39].

According to Fig. 31, after the first tunnel excavation, the ground settled by 11.4 mm. However, numerical modeling showed that the maximum settlement was 10.2 mm. The difference between these two measurements is 11%, and this percentage decreased by 2% after the excavation of the second tunnel. From this comparison, it can be concluded that the ground settlement profile is not symmetric after the excavation of the second tunnel. However, the shape of the pipeline settlement curve is symmetric after the excavation of both tunnels.

Fig. 32 displays the land subsidence profile due to step-by-step tunnel excavation. The negative horizontal axis represents the distance of the tunnel face before reaching the bottom of the pipe. Zero indicates the ground settlement when the tunnel is exactly under the pipeline, and positive shows the distance of the tunnel face after passing the pipeline location. Ground displacement increases with the progress of tunnel excavation. When the tunnel is placed 9 meters from the pipe location, ground settlement reaches a stable state with very little bending. Excavation of the second tunnel causes ground displacement to increase again and tilts the ground settlement curve towards the second tunnel. Major settlement occurs between -7.5 and 7.5 from the tunnel axis as shown in Fig. 32. Ground settlement reaches a stable state after +15 meters from the tunnel axis.

Fig. 33 illustrates the effect of asynchronous twin tunnel excavation on pipelines. The change in pipeline settlement is similar to ground settlement, with the difference that the settlement profile remains symmetrical after the second tunnel excavation. This difference depends on the axis-to-axis tunnel spacing (L) and their rigidity.

The effect of the axis to axis tunnel spacing (L) on the pipeline settlement profile is illustrated in Fig. 34. According to this figure, with the increase in tunnel spacing, the pipeline settlement profile changes from a V-shape to U and then W shape. The effect of this parameter on ground surface settlement is greater and faster than on pipelines. It should be noted that the shape of soil and pipe settlement depends on the relative stiffness of pipe and soil (K) as shown in Fig. 35. For a given tunnel spacing, by increasing the pipe-soil relative stiffness (K) the settlement of both pipeline and ground surface decreases. In addition, the pipeline settlement approaches a symmetrical profile, while the settlement profile of the ground surface remains asymmetric.

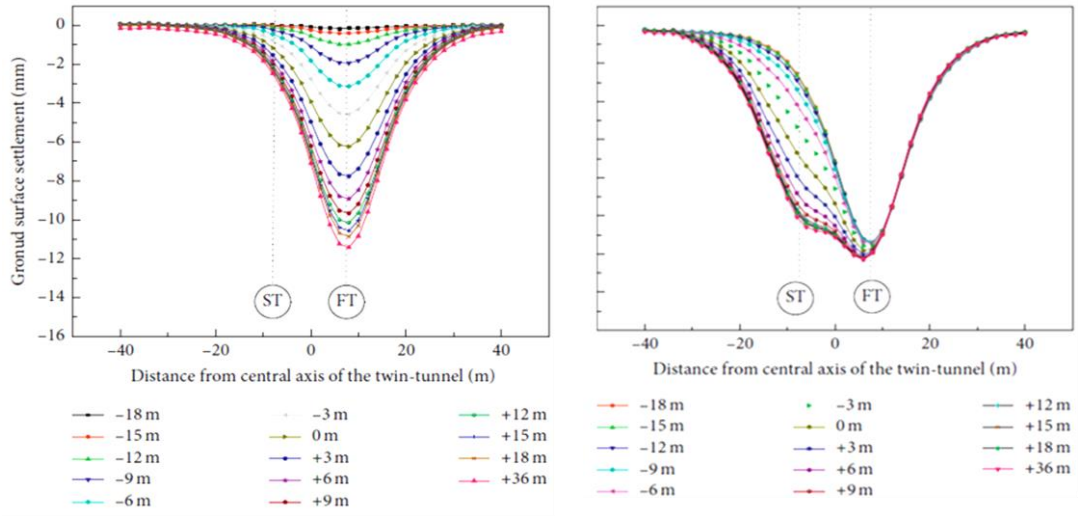

Fig. 32. Settlement profile due to step-by-step tunnel excavation [39].

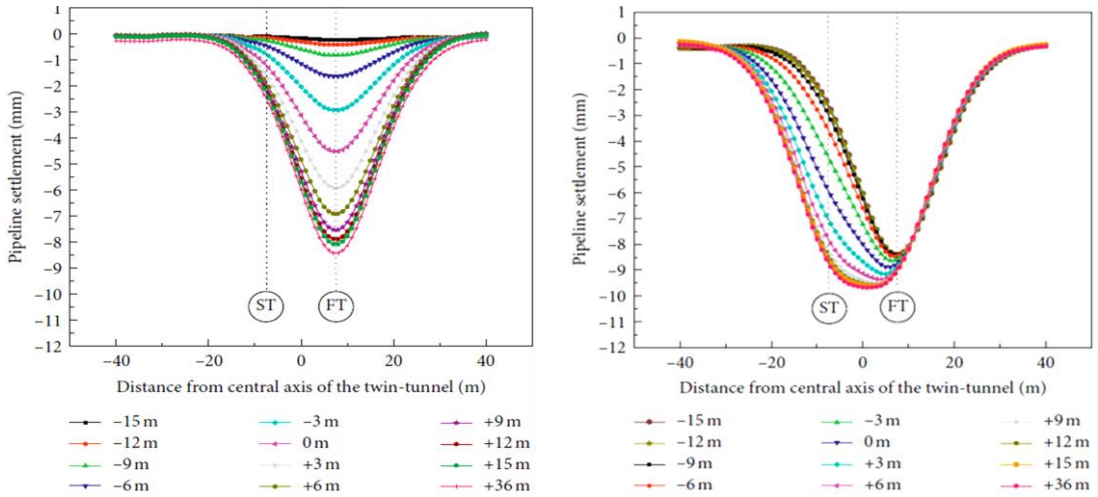

Fig. 33. Settlement of the pipeline during tunnel excavation [39].

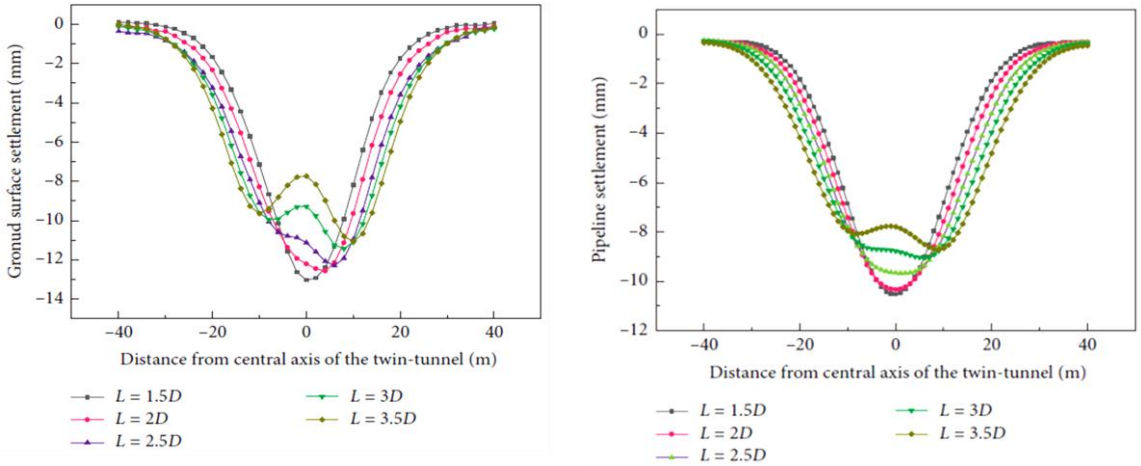

Fig. 34. The ground and pipeline settlement during tunnel excavation with different tunnel spacing [39].

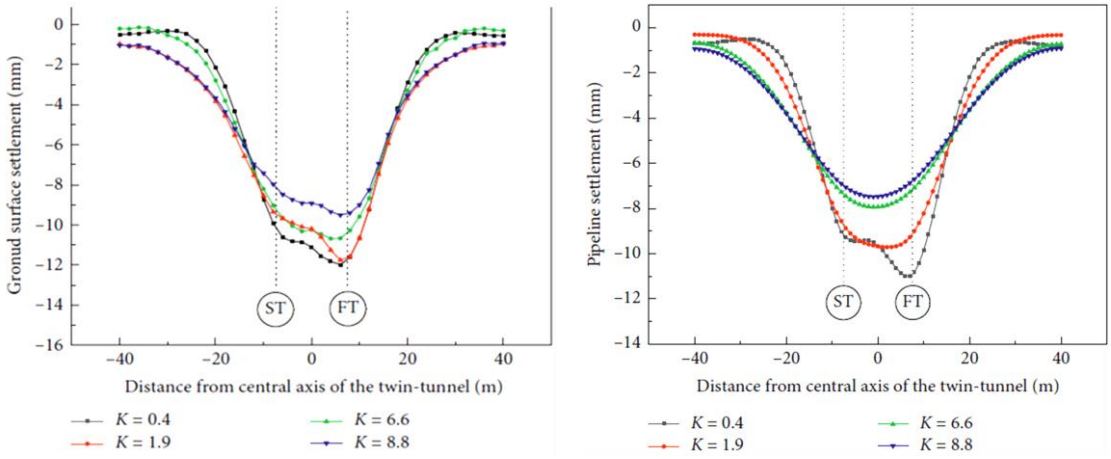

Fig. 35. The ground and pipeline settlement during tunnel excavation with different relative stiffness of pipe and soil [39]

7. CONCLUSIONS

Analytical solutions developed by Winkler (1867), Attewel et al. (1986), Klar et al. (2005), Vorster et al. (2005), and Klar and Marshall (2015) are less time-consuming and easier for practical application. However, these solutions idealize soil behavior as linear elastic and do not consider the effect of gap formation, soil stiffness degradation, and local yielding. Additionally, analytical solutions rely predominantly on Greenfield settlements to determine the pipeline's response. Nevertheless, no analytical solutions are available to predict tunneling-induced ground settlement while taking into account the pipeline's modification effect, gap formation, soil stiffness degradation, local yielding, and the effect of the pipeline's orientation concerning the tunnel alignment. Many researchers have used centrifuge and 1g physical models to solve these problems. However, these experimental methods are time-consuming, expensive, and require high precision and expertise. On the other hand, numerical methods require defining the appropriate behavioral model and input data despite their flexibility and applicability for different geometries and complex conditions of engineering problems. Each of the analytical, experimental, and numerical methods in solving the problem of soil-pipe interaction has deficiencies and limitations. Therefore, analytical, numerical, and experimental methods should be considered as the three main foundations of an engineering design, and none of them can replace the others. Based on the studies and review, the most important results are as follows:

The ground settlement profile follows a Gaussian curve. The inflection point (i) of this curve in clay soils is larger than in sandy soils, which means that the ground settlement profile is wider in the former than in the latter.

When the tunnel and pipeline are perpendicular to each other, five mechanisms related to soil-pipe interaction can be defined: global Greenfield soil settlement, gap formation below the pipe, positive down drag failure (when the pipe settles more than the soil), negative down drag failure (when the soil settles more than the pipe), and longitudinal interaction.

The maximum bending strain in the pipeline occurs when the tunnel and pipeline are perpendicular to each other. Additionally, the pipeline settlement is symmetrical when the tunnel and pipeline are perpendicular to each other.

When the pipe-soil relative stiffness increases, the pipe bending is less than the maximum soil bending.

At low tunnel convergences, the magnitudes of vertical and horizontal displacements are similar for all pipe tests and are relatively uniform throughout the depth of soil in the chimney zone. However, when the tunnel convergence increases, it causes a discontinuity in the displacement field.

Tunnel excavation causes different soil displacements when pipelines are used compared to when they are not used. If a tunnel is excavated under a pipeline with high stiffness, the pipeline's rigidity creates a resisting force against the ground. This results in less soil settlement than that of the flexible pipe.

Ground settlement, shear strain, and pipeline displacement are greater in flexible pipes than in rigid pipelines. This is due to the low resistance of flexible pipelines against bending and settlement caused by tunnel excavation.

The pipe bending can be positive or negative. Positive bending (downward) occurs near the tunnel axis, which is marked by sagging, but negative bending (upward) occurs at a distance from the tunnel axis, which is known as hogging.

The lowest bending occurred in the rigid pipe and the highest bending occurred in the flexible

pipe. The most bending changes in the pipes were related to the flexible pipe.

Tunneling can cause gap formation beneath pipelines, which can affect their bending behavior and loading conditions. The changes in gap height with tunnel convergence for three types of pipes (rigid, intermediate, and flexible) show that the flexible and intermediate pipes exhibit gap initiation at low tunnel convergence, while rigid pipes do not show gap formation until high convergence.

In twin tunnels excavation, the pipeline settlement profile changes from a V-shape to U and then W shape when the distance between the two tunnels' axis changes. The effect of this parameter on ground settlement is greater and faster than that on pipelines. It should be noted that the shape of soil and pipe settlement depends on the pipe-soil relative stiffness.

The material reviewed in this research will be efficient and useful for engineers who evaluate the soil-pipe interaction mechanism. Additionally, this study can help researchers interested in developing new analytical methods to overcome the limitations of the mentioned analytical methods and design and implement ideal experimental tests.

REFERENCES

[1] Hasanpour, R., Schmitt, J., Ozcelik, Y., Rostami, J. 2017. Examining the effect of adverse geological conditions on jamming of a single shielded TBM in Uluabat tunnel using numerical modeling. Journal of Rock Mechanics and Geotechnical Engineering, 9(6), pp.1112-1122.

[2] Zhao, C., Alimardani Lavasan, A., Barciaga, T., Schanz, T., 2018. Mechanized tunneling induced ground movement and its dependency on the tunnel volume loss and soil properties. The International Journal for Numerical and Analytical Methods in Geomechanics, 43(4), pp.781–800.

[3] 3. Mirsalari, S.E., Fatehi Marji, M. Gholamnejad, J., Najafi, M. 2017. A boundary element/finite difference analysis of subsidence phenomenon due to underground structures. Journal of Mining and Environment, 8 (2), pp.237-253.

[4] 4. Zhou, H., Gao, Y., Zhang, C., Yang, F., Hu, M., Liu, H., Jiang, Y., 2018. A 3D model of coupled hydro-mechanical simulation of double shield TBM excavation. Tunneling and Underground Space Technology, 71, pp.1-14.

[5] 5. Abdollahi, M.S., Najafi, M., Yarahmadi Bafghi, AR., Fatehi Marji, M. 2019. A 3D numerical model to determine suitable reinforcement strategies for passing TBM through a fault zone, a case study: Safaroud water transmission tunnel, Iran. Tunneling and Underground Space Technology, 88, pp.186-199.

[6] 6. Lui, B., Li, T., Han, Y., Li, D., He, L., Fu, C., Zhang, G., 2022. DEM-continuum mechanics coupling simulation of cutting reinforced concrete pile by shield machine. Computers and Geotechnics, 152, p.105036.

[7] 7. Terzaghi, K. 1943. Theoretical soil mechanics. John wiley & Sons, Inc, New York & London, 526p.

[8] 8. Tien, H.J., 1996. A literature study of the arching effect. M.Sc. Thesis, Massachusetts institute of technology, National Taiwan University.

[9] 9. Khosravi, M.H., Bahaaddini, M., Kargar, A.R., & Pipatpongsa, T. 2018. Soil arching behind retaining walls under active translation mode: review and new insights. International Journal of Mining and Geo-Engineering, IJMGE, 52(2), pp.131-140.

[10] 10. Khandouzi, G., Khosravi, M.H., 2023. Soil arching and ground deformation around tunnels in sandy ground, review and new insights. Journal of mining and environment, JME, https://doi.org/10.22044/jme.2023.13676.2532.

[11] 11. Khosravi, M.H., Pipatpongsa, T., & Takemura, J. 2016. Theoretical analysis of earth pressure against rigid retaining walls under translation mode. Soils and Foundations, 56(4), pp.664-675.

[12] 12. Khosravi, M. H., Hamedi Azad, F., Bahaaddini, M., & Pipatpongsa, T. 2017. DEM analysis of backfilled walls subjected to active translation mode. International Journal of Mining and Geo-Engineering, 51(2), pp.191-197.

[13] 13. Khosravi, M. H., Kargar, A. R., & Amini, M. 2020. Active earth pressures for non-planar to planar slip surfaces considering soil arching. International Journal of Geotechnical Engineering, 14(7), pp.730-739.

[14] 14. Khosravi, M.H., Sarfaraz, H., Pipatpongsa, T. & Sharifdeljuyi, A. 2022. Active Earth Pressure Distribution inside Narrow Backfill Considering Soil-Arching Effect. International Journal of Geomechanics, 22(7), p.06022013.

[15] 15. Sarfaraz, H., Khosravi, M.H., & Pipatpongsa, T. 2023. Theoretical and Numerical Analysis of Cohesive-Frictional Backfill against Battered Retaining Wall under Active Translation Mode. International Journal of Geomechanics, 23(6), p.04023079.

[16] 16. Khosravi, M. H., Sarfaraz, H., Esmailvandi, M., & Pipatpongsa, T. 2017. A numerical analysis on the performance of counterweight balance on the stability of undercut slopes. International Journal of Mining and Geo-Engineering, 51(1), pp.63-69.

[17] 17. Ukritchon, B., Ouch, R., Pipatpongsa, T., & Khosravi, M. H. 2018. Investigation of stability and failure mechanism of undercut slopes by three-dimensional finite element analysis. KSCE Journal of Civil Engineering, 22, pp.1730-1741.

[18] 18. Sarfaraz, H., Khosravi, M. H., Pipatpongsa, T., & Bakhshandeh Amnieh, H. 2021. Application of artificial neural network for stability analysis of undercut slopes. International Journal of Mining and Geo-Engineering, 55(1), pp.1-6.

[19] 19. Sarfaraz, H., Khosravi, M.H., Pipatpongsa, T. & Saedi, G. 2023. Estimation of passive earth pressure against a battered rigid retaining wall in cohesive-frictional backfill. Journal of Geomine, 1(1), pp.22-29.

[20] 20. Vorster, T. E. B. 2005. The effects of tunnelling on buried pipes. Ph.D. Thesis, Cambridge University.

[21] 21. Marshall, A.M., 2009. Tunneling in sand and its effect on pipelines and piles. Ph.D. Thesis, Department of Engineering, University of Cambridge, 270p.

[22] 22. Vorster, T.E., Klar, A., Soga, K. and Mair, R.J., 2005. Estimating the effects of tunneling on existing pipelines. Journal of Geotechnical and Geoenvironmental Engineering, 131(11), pp.1399-1410.

[23] 23. Klar, A., Marshall, A.M., Soga, K. and Mair, R.J., 2008. Tunneling effects on jointed pipelines. Canadian Geotechnical Journal, 45(1), pp.131-139.

[24] 24. Marshall, A.M., Klar, A. and Mair, R.J., 2010. Tunneling beneath buried pipes: view of soil strain and its effect on pipeline behavior. Journal of Geotechnical and Geoenvironmental Engineering, 136(12), pp.1664-1672.

[25] 25. Wang, Y., Wang, Q. and Zhang, K.Y., 2011. An analytical model for pipe-soil-tunneling interaction. Procedia Engineering, 14, pp.3127-3135.

[26] 26. Klar, A., Elkayam, I. and Marshall, A.M., 2016. Design oriented linear-equivalent approach for evaluating the effect of tunneling on pipelines. Journal of Geotechnical and Geoenvironmental Engineering, 142(1), p.04015062.

[27] 27. Shi, J., Wang, Y. and Ng, C.W., 2016. Three-dimensional centrifuge modeling of ground and pipeline response to tunnel excavation. Journal of Geotechnical and Geoenvironmental Engineering, 142(11), p.04016054.

[28] 28. Shi, J., Wang, Y. and Ng, C.W., 2016. Numerical parametric study of tunneling-induced joint rotation angle in jointed pipelines. Canadian Geotechnical Journal, 53(12), pp.2058- 2071.

[29] 29. Ma, S., Shao, Y., Liu, Y., Jiang, J. and Fan, X., 2017. Responses of pipeline to side-by- side twin tunnelling at different depths: 3D centrifuge tests and numerical modelling. Tunnelling and Underground Space Technology, 66, pp.157-173.

[30] 30. Shi, J., Zhang, X., Chen, L. and Chen, L., 2017. Numerical investigation of pipeline responses to tunneling-induced ground settlements in clay. Soil Mechanics and Foundation Engineering, 54, pp.303-309.

[31] 31. Klar, A., 2018. Elastic continuum solution for tunneling effects on buried pipelines using Fourier expansion. Journal of Geotechnical and Geoenvironmental Engineering, 144(9), p.04018062.

[32] 32. Lin, C., Huang, M., 2019. Tunneling-induced response of a jointed pipeline and its equivalence to a continuous structure. Soils and foundations, 59, pp.828-839.

[33] 33. Saboya, F., Jr., S. Tibana, R. M. Reis, A. D. Farfan, and C. M. D. A. R. Melo. 2020. Centrifuge and numerical modeling of moving traffic surface loads on pipelines buried in cohesionless soil. Transportation Geotechnics, 23, p.100340.

[34] 34. Guan, X., Zhang, L., Wang, Y., Fu, H., An, J., 2020. Velocity and stress response and damage mechanism of three types pipelines subjected to highway tunnel blasting vibration. Engineering Failure Analysis, 118, p.104840.

[35] 35. Lin, C., Huang, M., Nadim, F., Liu, Z., 2020. Tunnelling-induced response of buried pipelines and their effects on ground settlements. Tunnelling and underground space technology, 96, p.103193.

[36] 36. Xia, Y., Jiang, N., Zhou, C., Sun, J., Luo, X., Wu, T., 2021. Dynamic behaviors of buried reinforced concrete pipelines with gasketed bell-and-spigot joints subjected to tunnel blasting vibration. Tunnelling and underground space technology, 118, p.104172.

[37] 37. Yuan, S., Feng, D., Zhang, S., Lin, R., 2022. Support pressure assessment of tunnels in the vicinity of leaking pipeline using unified upper bound limit analysis. Computer and Geotechnics, 144, p.104662.

[38] 38. Xia, G., Liao, K., He, T., He, G., Liao, D. 2023. Numerical analyses of the stress and ultimate bearing capacity for small-diameter gas pipelines under multiple-wheel heavy vehicle. Journal of Pipeline Systems Engineering and Practice, 14(4).

[39] 39. Sun, S., Rong, C., Wang, H., Cui, L. and Shi, X., 2021. The ground settlement and the existing pipeline response induced by the nonsynchronous construction of a twin-tunnel. Advances in Civil Engineering, 2021, pp.1-12.

[40] 40. Marshall, A., Farrell, R., Klar, A., Mair, R., 2012. Tunnels in sands: the effect of size, depth and volume loss on Greenfield displacements. Géotechnique 62 (5), pp.385–399.

[41] 41. Zhou, B. 2014. Tunneling-induced ground displacements in sand. Ph.D. Thesis, University of Nottingham, 227 p.

[42] 42. Franza, A. 2016. Tunneling and its effects on piles and piled structures. Ph. D. Thesis, Department of Civil Engineering University of Nottingham, 279 p.

[43] 43. Franza, A., Marshall, A.M., Zhou, B., 2019. Greenfield tunnelling in sands: the effects of soil density and relative depth. Géotechnique, 69 (4), pp.297–307.

[44] 44. Franza, A., Marshall, A.M., Zhou, B., Shirlaw, N., Boone, S. 2019. Greenfield tunnelling in sands: the effects of soil density and relative depth. Géotechnique, 70(7), pp.639-646.

[45] 45. Moussaei, N., Khosravi, M.H., & Hossaini, M.F. 2019. Physical modeling of tunnel induced displacement in sandy grounds. Tunneling and Underground Space Technology, 90, pp.19-27.

[46] 46. Moussaei, N., Khosravi, M.H., & Hossaini, M.F. 2022. Physical modeling of soil arching around shallow tunnels in sandy grounds. International Journal of Mining and Geo-Engineering, IJMGE, 56(4), pp.413-422.

[47] 47. Khandouzi, G., & Khosravi, M.H. 2023. An analytical investigation of soil arching induced by tunneling in sandy ground. Tunneling and Underground Space Technology, 140, p.105242.

[48] 48. Franza, A., Marshall, A.M., 2019. Empirical and semi-analytical methods for evaluating tunneling-induced ground movements in sands. Tunneling and Underground Space Technology, 88, pp.47–62.

[49] 49. Lin, X.T., Chen, R.P., Wu, H.N., Cheng, H.Z., 2019. Three-dimensional stress-transfer mechanism and soil arching evolution induced by shield tunneling in sandy ground. Tunneling and Underground Space Technology. 93, p.103104.

[50] 50. Peck, B.B., 1969. Deep excavation and tunnelling in soft ground, State of the art volume. In 7th ICSMFE (Vol. 4, pp. 225-290).

[51] 51. O'Reilly, M.P. and New, B.M., 1982. Settlements above tunnels in the United Kingdom-their magnitude and prediction (No. Monograph).

[52] 52. Wang, Y., Wang, Q. and Zhang, K.Y., 2010. Tunneling effect on underground pipelines–a closed-form solution. Proceedings of Geotechnical Challenges in Megacities, Moscow, Russia, pp.814-819.

[53] 53. Wang, Z.X., Miu, L.C., Wang, R.R., Wang, F., Wang, X.L., 2014. Physical model tests and PFC3D modeling of soil-pipe interaction in sands during tunnelling. Chinese J. Geotech. Eng. 36 (1), pp.182–188 (in Chinese).

[54] 54. Wang, F., Du, Y.J., Yang, X., 2015. Physical modeling on ground responses to tunneling in sand considering the existence of HDPE pipes. Geotech Test. J. 38 (1), pp.85–97.

[55] 55. Jia, R.H., Yang, J.S., Ma, T., Liu, S.Y., 2009. Field monitoring and numerical analysis of shield tunneling considering existing tunnels. Chinese J. Geotech. Eng. 31 (3), pp.425–430.

[56] 56. Attewell, P.B., Yeates, J., Selby, A.R., 1986. Soil movements induced by tunnelling and their effects on pipelines and structures. Blackie & Son, London.

[57] 57. Klar, A., Vorster, T.E.B., Soga, K. and Mair, R.J., 2005. Soil—pipe interaction due to tunnelling: comparison between Winkler and elastic continuum solutions. Géotechnique, 55(6), pp.461-466.

[58] 58. Klar, A., Vorster, T., Soga, K., Mair, R., 2007. Elastoplastic solution for soil-pipe-tunnel interaction. J. Geotech. Geoenviron. Eng. 133 (7), pp.782–792.

[59] 59. Wang, Y., Shi, J. and Ng, C.W., 2011. Numerical modeling of tunneling effect on buried pipelines. Canadian Geotechnical Journal, 48(7), pp.1125-1137.

[60] 60. Guidelines for design steel pipe July 2001 "American lifelines alliance.

[61] 61. Klar, A. and Marshall, A.M., 2015. Linear elastic tunnel pipeline interaction: the existence and consequence of volume loss equality. Géotechnique, 65(9), pp.788-792.

[62] 62. Tsagareli, Z. V. 1965. Experimental investigation of the pressure of a loose medium on retaining walls with a vertical back face and horizontal backfill surface. Soil Mechanics and Foundation Engineering, 2(4), pp.197-200.

[63] 63. Khosravi, M. H., Pipatpongsa, T., Takahashi, A., & Takemura, J. 2011. Arch action over an excavated pit on a stable scarp investigated by physical model tests. Soils and foundations, 51(4), pp.723-735.

[64] 64. Khosravi, M., Tang, L., Pipatpongsa, T., Takemura, J., & Doncommul, P. 2012. Performance of counterweight balance on stability of undercut slope evaluated by physical modeling. International Journal of Geotechnical Engineering, 6(2), pp.193-205.

[65] 65. Khosravi, M. H., Pipatpongsa, T., & Takemura, J. 2013. Experimental analysis of earth pressure against rigid retaining walls under translation mode. Géotechnique, 63(12), pp.1020-1028.

[66] 66. Salehi Alamdari, N., Khosravi, M. H., & Katebi, H. 2020. Distribution of lateral active earth pressure on a rigid retaining wall under various motion modes. International Journal of Mining and Geo-Engineering, 54(1), pp.15-25.

[67] 67. Khatami, H.R., Deng, A., Jaksa, M., 2019. An experimental study of the active arching effect in soil using the digital image correlation technique. Computers and Geotechnics. 108, pp.183–196.

[68] 68. Khandouzi, G., Khosravi, M.H., Mahmudi, H. 2023. Experimental investigation of the relationship between tunnel volume loss and soil arching in sandy ground. The 5th International Underground Excavations Symposium, Istanbul. Pp.785-796.

[69] 69. Khosravi, M. H., Takemura, J., Pipatpongsa, T., & Amini, M. 2016. In-flight excavation of slopes with potential failure planes. Journal of Geotechnical and Geoenvironmental Engineering, 142(5), p.06016001.

[70] 70. Khosravi, M. H., Pipatpongsa, T., Takemura, J., & Amini, M. 2017. Influence of modeling material on undercut slope failure mechanism. Journal of Mining and Environment, 8(4), pp.645-662.

[71] 71. Song, G.Y., Marshall, A.M., 2020. Centrifuge modelling of tunnelling induced ground displacements: pressure and displacement control tunnels. Tunnelling and Underground Space Technology. 103, p.103461.

[72] 72. Nasiri, F., Khosravi, M. H., & Takemura, J. 2022. An experimental study of pile stabilized infinite slopes under in-flight pseudo-static loading. Bulletin of Engineering Geology and the Environment, 81(10), p.440.

[73] 73. Marshall, A.M., Elkayam, I., Klar, A. and Mair, R.J., 2010, June. Centrifuge and discrete element modelling of tunnelling effects on pipelines. In Proceedings of the 7th International Conference on Physical Modelling in Geotechnics,pp. 633-637.

[74] 74. Marshall, A.M. and Mair, R.J., 2008. Centrifuge modelling to investigate soil-structure interaction mechanisms resulting from tunnel construction beneath buried pipelines. In Geotechnical aspects of underground construction in soft ground (pp. 719-724). CRC Press.

[75] 75. Aljaberi, M., Elshesheney A., Mohamed, M., Sheehan, T., 2024. Experimental investigation into the effects of voids on the response of buried flexible pipes subjected to incrementally increasing cyclic loading. Soil Dynamics and Earthquake Engineering, 176, p.108268.